USING FE-S-SI INTERNAL STRUCTURE MODELS TO STUDY MERCURY'S INTERIOR. A. H. Dunnigan[1,2], K. M. Soderlund[3], D. Liu[3], G. Steinbrügge[4], A. Rivoldini[5], M. Dumberry[6], G. Schubert[7], H. Cao[7,8], D. M. Schroeder[9] [1]Department of Physics and Astronomy, University of North Carolina at Chapel Hill, [2]Lunar and Planetary Institute (USRA), [3]Institute for Geophysics, Jackson School of Geosciences, University of Texas at Austin, [4]NASA Jet Propulsion Laboratory, California Institute of Technology, [5]Royal University of Belgium, [6]Department of Physics, University of Alberta, Edmonton, [7]Department of Earth, Planetary, and Space Sciences, University of California Los Angeles, [8]Department of Earth and Planetary Sciences, Harvard University [9]Department of Geophysics, Stanford University.

Introduction: The Mercury Surface, Space, Environment, Geochemistry, and Ranging (MESSENGER) mission provided new geodetic and magnetic measurements we can use to constrain the planet's internal structure and test hypotheses for how its magnetic field is generated and maintained.

Two geodetic constraints (among others) that we consider are the normalized moment of inertia $\tilde{C}$ and the ratio C_m/C, where C is the polar moment of inertia and C_m is the polar moment of inertia of the solid part of Mercury involved in libration. Libration corresponds to the change in Mercury's spin frequency caused by the 88-day, periodically reversing solar torque and has an amplitude denoted by ϕ_0. If $C_m = C$, the core is solid and the whole planet librates as a single body. If $C_m < C$, the core is partially fluid. $\tilde{C}$ on the other hand, shows how centrally concentrated the interior of the planet is. Margot et al. (2012) [1] obtained $\tilde{C} = 0.346 \pm 0.014$, $C_m/C = 0.426 \pm 0.045$, and $\phi_0 = 38.5 \pm 1.6$ arcsec, while Genova et al. (2019) [2] obtained $\tilde{C} = 0.333 \pm 0.005$, $C_m/C = 0.443 \pm 0.007$, and $\phi_0 = 40.0 \pm 2.9$ arcsec (1σ error). The libration amplitudes indicate that the core is at least partially liquid; both $\tilde{C}$ values also indicate the possibility of a solid inner core, with lower values implying a larger inner core as more mass is concentrated towards the center [3].

We can also constrain the interior of Mercury using its magnetic field. Mercury's magnetic field is about 100 times weaker at the surface than Earth's magnetic field with a topology well characterized by an axisymmetric dipole that is offset northward [4]. With the detection of magnetized rocks on Mercury's surface by MESSENGER, there is evidence of an ancient magnetic field as well [5]. Dynamo action is the leading hypothesis to sustain this field, indicating that convection of an electrically conducting fluid must be present both today and early in the planet's history.

Given Mercury's small size and the likely prevalence of light elements in its core, iron snow is a potential driver of thermocompositional convection within the liquid core [6]. In this crystallization scenario, snow zones are formed when Fe-rich solids precipitate in the outer core fluid when the temperature drops below the liquidus, sink under gravity, and thus drive thermocompositional convection upon re-melting at depth to power Mercury's dynamo.

We build upon prior theoretical interior structure models of Mercury [3][6] that have used both Fe-S and Fe-Si end-member core compositions. Steinbrügge et al. (2021) discusses the newer MOI constraint $\tilde{C} = 0.333 \pm 0.005$ [2] applied to the models which presents some challenges to our understanding of Mercury's interior, in particular high core-mantle boundary (CMB) temperatures and low mantle densities [3].

Methods: In this study, we focus on present-day models of the internal structure, assuming an Fe-S-Si core composition as suggested by geochemistry [7] and matching geodetic constraints such as $\tilde{C} = 0.346 \pm 0.014$, $C_m/C = 0.426 \pm 0.045$, and $\phi_0 = 38.5 \pm 1.6$ arcsec [1]. The models are spherically symmetric, with layers that include a potential solid inner core, liquid outer core that may develop snow regions, mantle, and crust. The models integrate pressure, gravity, density, and temperature profiles radially outwards from the core, to the core-mantle boundary (CMB), and to the crust [3] at radial increments of 50 km. The models have two free parameters at different inner core radii, wt % Si and wt % S. We assume that wt % Si is constant with radius, and we invert wt % S. Models are produced for concentrations from 1-12 wt % Si (i.e. up to the eutectic [8]), where each wt % Si value supports different inner core radii as long as they fit within the geodetic constraints.

Results: To illustrate the range of internal properties the present-day models may have, we created contour plots of snow zone presence, CMB temperature, CMB pressure, mean mantle density, core mass, S concentration averaged throughout the core, and S concentration at the inner core boundary (ICB). Each plot has a y-axis of inner core radius and x-axis of silicon concentration. Each point on a plot is a present-day model with its own inner core radius and silicon concentration. There is a general trend of higher silicon concentrations yielding larger inner core radii, which occurs because the models must match geodetic constraints like $\tilde{C}$. The snow zone contour plot (shown

in Fig. 1) is perhaps the most telling, as it shows which models contain iron snow. The lowest Si concentrations support snow zones at all inner core radii, while higher Si concentrations only support snow zones at some of the largest inner core radii. If we assume that Mercury's dynamo is supported by the power generated by the remelting of iron-rich snow, then we can focus on the models that have snow zones specifically.

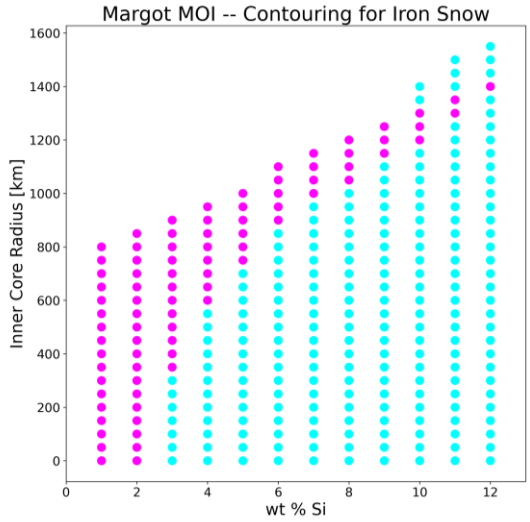

Fig. 1. Inner core radius vs Si concentration, where each point represents a present-day model that satisfies $\tilde{C} = 0.346$ [1]. The plot is contoured by whether there is the presence of a snow zone (magenta) or not (cyan).

By focusing in on the present-day models with snow zones, we can find realistic ranges for all of the properties that we contoured for. These ranges are shown in Tab. 1. Comparing these to the total ranges shown in the contour plots, we expect to see higher CMB pressures and S concentrations averaged throughout the core, and lower mantle densities and core masses. CMB temperature and S concentration at the ICB are more constrained around the median of each total range.

Internal Property	Range [Units]
CMB Temperature	1440-1910 [K]
CMB Pressure	5.13-5.29 [GPa]
Mantle Density	3310-3430 [kg/m^3]
Core Mass	(5.80-5.83) x 10^{22} [kg]
S Concentration (ICB)	0.06-0.10 [wt %]
S Concentration (Core Average)	0.05-0.10 [wt %]

Tab. 1. Internal property estimates when assuming Fe-S-Si core composition models, $\tilde{C} = 0.346$ [1], and that snow zones exist at present-day.

Conclusion: By constructing Fe-S-Si core composition models to match geodetic constraints [1][2] and placing further constraints based off of assumptions about Mercury's magnetic field, we can infer properties of its interior. These ranges can also be compared to additional estimates and assumptions to potentially further constrain Mercury's interior. For example, a single snow layer that extends to the CMB is not expected to support a dynamo, so excluding models in which this occurs can further constrain the interior.

Now that we have constrained ranges for Mercury's interior properties when meeting the Margot et al. (2012) geodetic constraints, we can take the results further. In a next step we can reproduce the contour plots for present-day models that meet the more recent estimate of $\tilde{C} = 0.333 \pm 0.005$ [2]. We can compare our current results to the new ones, as well as compare them to prior interior model results [3][6]. By incorporating the newer geodetic constraints [2], we can test if updated models run into new or similar challenges.

Acknowledgments: This work was supported by the Summer Undergraduate Program for Planetary Research and the LPI Cooperative Agreement. This work has also been funded by NASA grant number 80NSSC19K0793. M. Dumberry is supported by an NSERC/CRSNG Discovery Grant. A. Rivoldini was financially supported by the Belgian PRODEX program managed by the European Space Agency in collaboration with the Belgian Federal Science Policy Office.

References: [1] Margot J. L. et al. (2012) Mercury's moment of inertia from spin and gravity data. *Journal of Geophysical Research: Planets*, 117(E12). [2] Genova A. et al. (2019) Geodetic evidence that Mercury has a solid inner core. *Geophysical Research Letters*, 46(7):3625-3633. [3] Steinbrügge G. et al. (2021) Challenges on Mercury's interior structure posed by new measurements of its obliquity and tides. *Geophysical Research Letters*, 48(3):e2020GL089895. [4] Anderson B. J. et al. (2011) The global magnetic field of Mercury from MESSENGER orbital observations. *Science* 333.6051 (2011): 1859-1862. [5] Johnson C. et al. (2015) Low-altitude magnetic field measurements by messenger reveal Mercury's ancient crustal field. *Science*, 348(6237):892-895. [6] Dumberry M. and Rivoldini A. (2015) Mercury's inner core size and core-crystallization regime. *Icarus*, 248:254-268. [7] Chabot et al. (2014) Experimental constraints on mercury's core composition. *Earth and Planetary Science Letters*, 390:199–208. [8] Edmund E. et al. (2022) The Fe-FeSi phase diagram at Mercury's core conditions. *Nature Communications*, 13(1):1–9.